First metallicity determination from near-infrared spectra for five obscured Cepheids discovered in the inner disc

L. Inno [1] M. A. Urbaneja,[2] N. Matsunaga,[3] G. Bono,[4,5] M. Nonino,[6] V. P. Debattista,[7] M. C. Sormani,[8] M. Bergemann,[1] R. da Silva,[5,9] B. Lemasle,[10] M. Romaniello[11] and H.-W. Rix[1]

[1]*Max-Planck Institute for Astronomy, D-69117 Heidelberg, Germany*
[2]*Institut für Astro- und Teilchenphysik, Universität Innsbruck, Technikerstr 25/8, A-6020 Innsbruck, Austria*
[3]*Department of Astronomy, School of Science, The University of Tokyo, 7-3-1 Hongo, Bunkyo-ku, Tokyo 113-0033, Japan*
[4]*Dipartimento di Fisica, Università di Roma Tor Vergata, via della Ricerca Scientifica 1, I-00133 Rome, Italy*
[5]*INAF-Osservatorio Astronomico di Roma, via di Frascati 33, Monte Porzio Catone (Roma), Italy*
[6]*INAF-Oss. Astr. di Trieste, Via Tiepolo 11, I-34131 Trieste, Italy*
[7]*Jeremiah Horrocks Institute, University of Central Lancashire, Preston PR1 2HE, UK*
[8]*Zentrum für Astronomie, Institut für theoretische Astrophysik, Universität Heidelberg, Albert-Ueberle-Str 2, D-69120 Heidelberg, Germany*
[9]*Agenzia Spaziale Italiana, via del Politecnico snc, I-00133 Rome, Italy*
[10]*Astronomisches Rechen-Institut, Zentrum für Astronomie der Universität Heidelberg, Mönchhofstr 12-14, D-69120 Heidelberg, Germany*
[11]*European Southern Observatory, Karl-Schwarzschild-Str 2, D-85748 Garching bei Munchen, Germany*

ABSTRACT

We report the discovery of five new classical Cepheids located in the inner Galactic disc at longitude $l \simeq -40°$ in our IRSF/SIRIUS near-infrared (NIR) variability survey. The new Cepheids are unique in probing the kinematics and metallicity of young stars at the transition between the inner disc and the minor axis of the central bar, where they are expected to be less affected by its dynamical influence. This is also the first time that metallicity of Cepheids is estimated on the basis of medium-resolution ($R \sim 3000$) NIR spectra, and we validated our results with data in the literature, finding a minimal dependence on the adopted spectroscopic diagnostics. This result is very promising for using Cepheids as stellar proxy of the present-time chemical content of the obscured regions in the disc. We found that the three Cepheids within 8–10 kpc from us have metallicities consistent with the mean radial metallicity gradient, and kinematics consistent with the Galactic rotation curve. Instead, the closest ($\sim$4 kpc)/farthest ($\sim$12 kpc) Cepheids have significant negative/positive residuals, both in velocity and in iron content. We discuss the possibility that such residuals are related to large-scale dynamical instabilities, induced by the bar/spiral-arm pattern, but the current sample is too limited to reach firm conclusions.

Key words: stars: variables: Cepheids – Galaxy: abundances – Galaxy: kinematics and dynamics.

1 INTRODUCTION

A comprehensive empirical characterization of the present-time Milky Way (MW) disc is pivotal to pursue a full understanding of the formation history of our Galaxy. While the structure of its central components, such as the bar and the bulge, have been recently unveiled by large-scale surveys, their dynamical interplay and their mixing with the underlying disc-component remains poorly understood. The inner disc (ID), defined as the region within a Galactocentric distance (R_{GC}) from 4 to 7 kpc (Feltzing & Chiba 2013), is

the Galactic locus where all these components coexist and, likely, interact. On the basis of stellar counts and photometric surveys, it is now well established that within the ID lies the interface between the disc, its inner spiral-arms and the long bar, with a half length of $\sim$5 kpc (see e.g. Bland-Hawthorn & Gerhard 2016, for a recent review on the Galactic bar and bulge), but it is still unclear e.g. where the bars' ends and resonances are located (Benjamin et al. 2005), whether there is a central molecular ring (Heyer & Dame 2015) and which mechanism triggers the intense star-forming activity found e.g. in W43 (Bally et al. 2010), etc.

Moreover, the ID is expected to be strongly affected by the bar-driven dynamical instabilities (Rix & Bovy 2013), which impact both its kinematics and the chemical enrichment, and therefore the

* E-mail: inno@mpia-hd.mpg.de

observed radial metallicity gradient. Indeed, gas-phase metallicity gradients in barred external galaxies are systematically shallower than the ones in un-barred galaxies, as supported by empirical (e.g. Zaritsky, Kennicutt & Huchra 1994; Allard et al. 2006) and theoretical investigations (e.g. Athanassoula 1992; Friedli & Benz 1995; Minchev, Chiappini & Martig 2013), while the stellar phase shows a higher degree of complexity (e.g. Sánchez-Blázquez et al. 2011). In the generally accepted inside-out infall scenario of the Galactic disc evolution (Chiappini, Matteucci & Gratton 1997), the radial migration induced by the bar's instabilities produces a smoothing of the metallicity content in the ID. At the same time, the bar's resonances allow a pile-up of fresh material from inflowing gas, which produces hotspots of star formation activity, where local enrichment can occur. The end-product of this mechanism is the presence of an azimuthal metallicity gradient (e.g. Khoperskov et al. 2018, and reference therein).

Despite the relevance of the role played by the ID in the Galactic evolution, its kinematics and chemical content has not been empirically constrained yet, as a consequence of the significant dust extinction towards the Galactic plane, which makes observations challenging at low latitudes. There are a few studies based on bright hot stars (e.g. OB stars, Daflon & Cunha 2004), while more investigations focused on the use of star clusters (e.g. Jacobson et al. 2016) to trace the chemical pattern of the inner Galaxy.

In this context, cassical Cepheids are the best-suited stellar probes, as they are so luminous that can be seen at distances larger than 8 kpc from us, even though substantive dust extinction, and their individual distances and ages can be precisely determined on the basis of their pulsation periods. They are very young stars (ages $\lesssim 200$ Myr Bono et al. 2005), but they have lower effective temperature ($T_{\mathrm{eff}} \sim 6000\,\mathrm{K}$) with respect to other stars of similar age and hence their spectra, rich in metal absorption lines, allow for precise abundance determinations of many different chemical elements (e.g. da Silva et al. 2016, and references therein).

Indeed, works based on the chemical abundances of Cepheids within 4–7 kpc from the Galactic Centre, have shown that the metallicity gradient steepens in the ID (Andrievsky et al. 2002; Pedicelli et al. 2010; Luck et al. 2011; Genovali et al. 2013), and it can reach super-solar metallicity of ~ 0.4 dex at $R_{\mathrm{GC}} \sim 2.5$ kpc (Martin et al. 2015; Andrievsky et al. 2016). However, such investigations rely on only a few Cepheids (~ 5) at galactocentric radius of $\lesssim 5$ kpc, and thus at the transition with the bar.

In fact, the number of Cepheids currently known in inner regions of the disc (Metzger & Schechter 1998, fig. 11) is still limited with respect to the ones found in the solar neighbourhood, because variability surveys, traditionally performed in the optical bands, were strongly hampered by dust extinction towards the Galactic Centre. Even the ongoing *Gaia* space mission will suffer from severe limitations in the Galactic plane, where its capability of detecting variables brighter than ~ 20 mag (G band), will translate to distances $\lesssim 6$ kpc due to extinction (Windmark, Lindegren & Hobbs 2011). Near-infrared (NIR) variability surveys have instead the capability to probe the innermost regions of the Galaxy by overcoming the thorny problems of the high extinction and the differential reddening.

In particular, our NIR survey towards the Galactic plane (Matsunaga et al. 2011), started in 2007 at the Japanese Infrared Survey Facility (IRSF), pioneered the search for distant Cepheids in the NIR bands and led to the discovery of four new Cepheids located in the nuclear bulge (Matsunaga et al. 2011, 2015), 13 new Cepheids beyond the Galactic Centre (Matsunaga et al. 2016) and three new Cepheids within $R_{\mathrm{GC}} = 3-5$ kpc in the Northern ID (Tanioka et al.

2017). At the same time, NIR data collected by the ESO public survey VVV (VISTA survey of the Via Lactea Minniti et al. 2010) also reported the discovery of additional 24 Cepheids located beyond the GC (Dékány et al. 2015a,b). However, determining the chemical abundances of the Cepheids identified by such NIR surveys also requires the use of NIR spectroscopy, which remains challenging for dynamical supergiant stars like Cepheids. In fact, while abundance determination of Cepheids based on optical spectra is well established, the NIR regime is still in its infancy, and a very limited background study is available in the literature (see e.g. Sasselov & Lester 1990; Nardetto et al. 2011).

In this paper, we report the discovery of five new Cepheids located in the ID, at longitudes ~ -40 deg and close to the minor axis of the central bar. As a follow up of the photometric observations, we collected medium-resolution ($R \sim 3000$) NIR spectra with ISAAC@VLT for all the new Cepheids and we were able to determine their kinematics and iron abundances. The new Cepheids are the first ever detected in this region of the disc and allow us to investigate the kinematics and chemical content of young stars in such crucial transition region.

The paper is organized as follows. In Section 2, we describe our photometric survey, the photometric data and data-reduction, and we present the NIR light curves of the new Cepheids, together with their distance estimates (Section 3). Then, we describe the spectroscopic data set in Section 4, and the analysis techniques for optical and NIR spectra, including the calibration of an homogenous metallicity abundance scale and the determination of the Cepheids' velocities. We investigate the kinematics of the new Cepheids in the ID in Section 5, and their metallicity as a function of galactocentric radius (Section 6.1) and azimuthal angle (Section 6.2). Finally, in Section 7, we summarize and discuss our results in the context of the Galactic disc evolution.

2 DETECTION AND CLASSIFICATION OF THE NEW CEPHEIDS

We conducted an NIR survey in the Galactic plane towards the line of sights $l = -20°$, $-30°$, and $-40°$ with the IRSF 1.4 m telescope and the SIRIUS camera, which takes images in the three NIR bands J (1.25 µm), H (1.64 µm), and K_{S} (2.14 µm) simultaneously (Nagashima et al. 1999; Nagayama et al. 2003). The instrumental field of view is about 7.7 arcmin $\times$ 7.7 arcmin, with a pixel scale of 0.45 arcmin pix^{-1}. Between 2007 and 2009, 30–40 observations have been performed for nine fields along the selected lines of sight. For each direction, we carried out monitoring observations for a 20 arcmin $\times$ 20 arcmin area, covered by a 3 $\times$ 3 IRSF/SIRIUS fields of view. To obtain the photometry of the stars in these fields, we applied the same analysis presented in Matsunaga et al. (2009). After the pipeline reduction we carried out point spread function fitting photometry using the DAOPHOT (Stetson 1987) package in IRAF.[1] Among all the images collected in each filter, the one characterized by the best condition (sky transparency and seeing) was selected as a reference frame for all the other observations of the same field. The photometric results of this reference frame were compared with the 2 Micron All-sky Survey point source catalogue (Skrutskie et al. 2006) in order to standardize the magnitudes. The

---

[1]IRAF – Imaging Reduction and Analysis Facility – is distributed by the National Optical Astronomy Observatory, which is operated by the Association of Universities for Research in Astronomy, Inc., under cooperative agreement with the National Science Foundation http://iraf.noao.edu/

reference frame has then been adopted to calibrate the remaining images of the same field. Thus, we created a master list of objects detected in each image, and we searched for their variability by adopting the same technique described in Matsunaga et al. (2013). This technique identifies the stars for which the variation in magnitude is larger than three times the standard deviation computed on all the images of the same object in a given filter. Among the many variable stars discovered (∼100, Matsunaga et al. in preparation), we found five objects for which the light-curve shape is compatible with the ones of classical Cepheids. These Cepheids are the first ones ever detected in the IV Galactic quadrant ($-90 \leq l \leq 0°$) and in the ID, and thus have been renamed ID-1, ID-2, ID-3, ID-4, and ID-5, in order of increasing right ascension.

We estimated the period P of the new identified Cepheids by adopting the multiband generalized periodogram (VanderPlas & Ivezić 2015) and fitting the photometric data with a fourth-order Fourier series. On the basis of the peak width in the periodogram, we estimate a precision of ±0.005 d on the period determination (VanderPlas 2018). The J-, H-, and K_S-band light curves of the new Cepheids together with their analytical fits are shown in Fig. 1 (ID-1: purple, ID-2: orange, ID-3: magenta, ID-4: cyan, ID-5: lime) and the resulting flux-averaged magnitudes in each band, indicated by the subscript F, are listed in Table 1. The error bars show the photometric errors, which range from $e_J \sim 0.01$ mag (at $J \sim 11$ mag) to $e_J \sim 0.1$ mag (at $J \sim 16$ mag). We also performed a template fit (red lines in Fig. 1), by using the method and templates described in Inno et al. (2015, 2016) and obtained their intensity-scaled mean magnitudes and associated errors, indicated by the subscript T in Table 1. The difference in the resulting mean magnitudes between the two methods is lower than 0.1 per cent but the template-fitting is less sensitive to spurious features in the shape of the light curves introduced by the photometric noise. Moreover, the templates are less flexible than the truncated Fourier series, because the fit is performed on just three free parameters: amplitude, mean magnitude and phase shift. Thus, the low chi-squared (Table 1) of the best fit further supports the classification of the new variables as classical Cepheids.

In fact, the J-band light curves of the new Cepheids show indeed features typical of known classical Cepheids with similar periods, such as e.g. the appearance of a bump on the rising branch related to the so-called Hertzsprung Progression starting at period ≥7 d (Bono, Castellani & Marconi 2002). In order to properly quantify these proprieties, we determined the Fourier parameters of the J-band light curves: $A_1, R_{21}, R_{31}, \Phi_{21}, \Phi_{31}$ as defined by Simon & Lee (1981). These parameters are listed in Table 2 and shown in Fig. 2, where they are compared to the ones of known Cepheids in the MW (Laney & Stobie 1992; Monson & Pierce 2011, dark dots), as well as in the Large (Persson et al. 2004, light grey squares) and in the Small Magellanic Cloud (Inno et al. 2015, grey diamonds). Unfortunately, extensive data sets of J-band light curves for Type 2 Cepheids are not available in the literature, thus it is difficult to obtain accurate Fourier parameters of these variables. However, we included the available data for Type 2 Cepheids towards the Galactic Centre (Matsunaga et al. 2013, purple triangles), and in the Large Magellanic Cloud (LMC; Macri et al. 2015; Bhardwaj et al. 2017, yellow triangles) and we found an overlap of the Fourier parameters for population 1 and 2 Cepheids, as also seen in the optical (Soszyński et al. 2018). Thus, we cannot exclude a misclassification only on the basis of the Fourier parameters. However, by taking into accounts the results from the template fitting, the light-curve shape and the consistency of the distance and extinction values discussed in the next section, such misclassification seems unlikely.

3 DISTANCE DETERMINATION OF THE NEW CEPHEIDS

The multiwavelength observations of the new Cepheids allow for a simultaneous determination of their distances and extinction by using period–luminosity (PL) relations in two different bands and by computing the corresponding selective extinction coefficients on the basis of the assumed extinction law. However, recent works (e.g. Majaess et al. 2016; Nataf et al. 2016; Schlafly et al. 2016) have shown that the extinction law in the MW is patchy and can vary as a function of the line of sight, even in the NIR regime. Such uncertainty on the adopted extinction law strongly impacts Cepheids' distance determinations, especially in highly obscured Galactic regions, as extensively discussed e.g. in Matsunaga et al. (2018). As described in Tanioka et al. (2017), we can use the extinction laws by Cardelli, Clayton & Mathis (1989, hereinafter C89) and by Nishiyama et al. (2006, hereinafter N06) to determine our best estimates of the Cepheids' distances and the likely maximum uncertainties. In fact, the published values of the exponent α for the power law used to model the extinction, mostly range between the two values determined by these two authors, namely 1.61 (C89) and 1.99 (N06).

We use a similar approach here: in order to determine the true distance modulus and extinction, we adopt the PL relations in the H and K_S bands estimated by Inno et al. (2016) for the LMC Cepheids, calibrated by assuming a mean distance modulus to the LMC of $18.493 \pm 0.008 \pm 0.047$ mag (Pietrzyński et al. 2013) and transformed into the IRSF photometric system (Kato et al. 2007).

In fact, the true distance modulus, defined as

$$\mu_0 = \mu_{K_S} - A_{K_S} \qquad (1)$$

can be derived on the basis of the apparent distance modulus in the H and K_S bands: $\mu_{K_S} = \langle K_S \rangle - \langle M(K_S) \rangle$, $\mu_H = \langle H \rangle - \langle M(H) \rangle$, where $M(K_S)$ and $M(H)$ are computed on the basis of the adopted PL relations, and the selective absorption in the K_S band is obtained from the following equation:

$$A_{K_S} = A_{K_S}/E(H - K_S) \times (\mu_H - \mu_{K_S}), \qquad (2)$$

by assuming first the coefficient $A_{K_S}/E(H - K_S) = 1.83$ by C89, and then $A_{K_S}/E(H - K_S) = 1.44$ by N06.

The distance modulus obtained for the same Cepheids with the different extinction laws are listed in columns 2 and 4 of Table 3 and they differ from 0.2 mag (ID-1,4) up to 0.4 mag (ID-2,3), or 16 per cent in distance. This difference is then adopted as the *conservative* estimate of the systematic uncertainty on our distance determination.

3.1 Comparison with available dust maps and best distance estimates

In order to determine the best distance estimates, we compare the distance modulus obtained by using the two different extinction laws with the one predicted on the basis of a three-dimensional dust map. In fact, Drimmel, Cabrera-Lavers & López-Corredoira (2003) computed such a map for the fourth Galactic Quadrant, where the new Cepheids are located, and Bovy et al. (2016, hereinafter B16) incorporated it in a comprehensive Galactic extinction map. Thus, we used the B16 *mwdust* code to determine the amount of selective absorption in the visual band for the five line of sights where the new Cepheids are located and at different distances.

Note that the dust map computed by Drimmel et al. (2003) rely on the dust emission in the Far-Infrared as measured by the
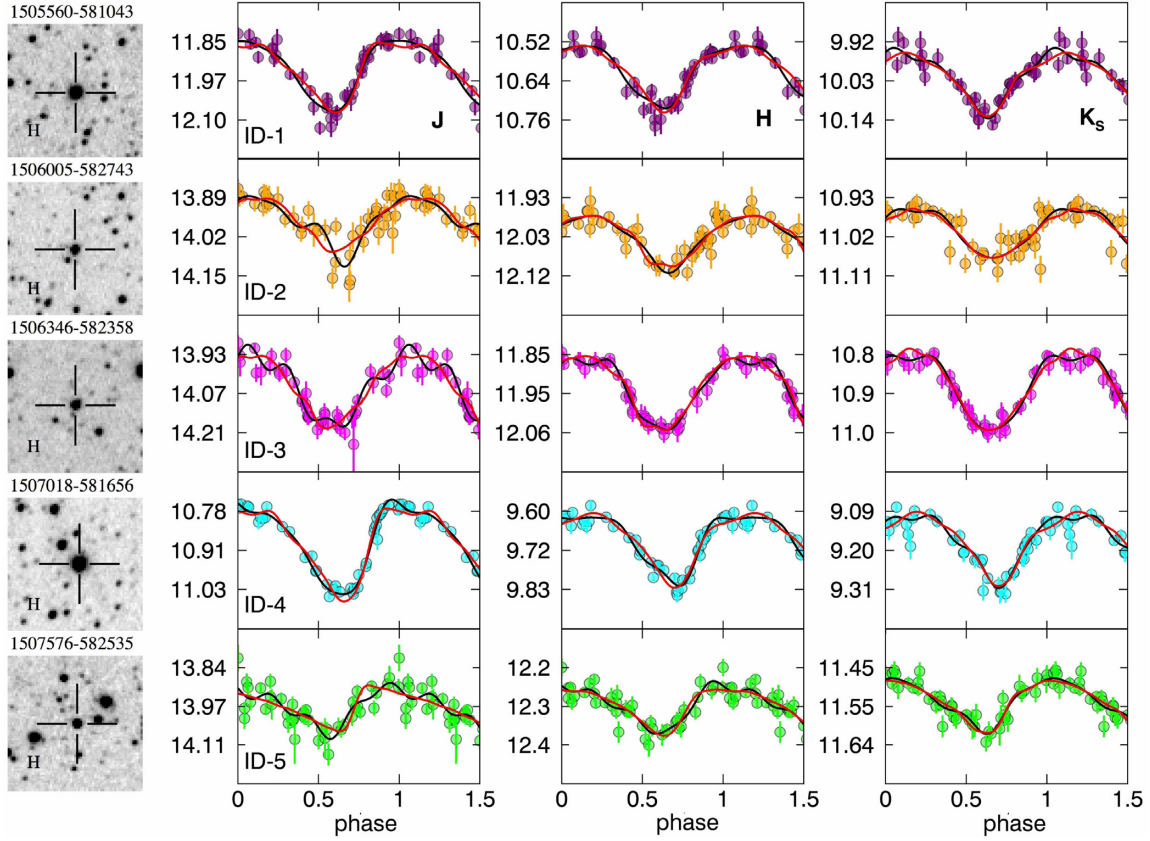
Figure 1. From top to bottom: observed light curves in the J, H, and K_S band for the five newly discovered Cepheids (ID-1: purple; ID-2: orange; ID-3: magenta; ID-4: cyan; ID-5: lime) interpolated by the fourth-order Fourier series best fit (black line) and the template light curves (red line, Inno et al. 2015). The error bars are the photometric error associated with the observed magnitude, while the typical rms ranges from 0.05 (ID-5) to 0.08 mag (ID-3) in the K_S band.

COBE/DIRBE mission, on an assumed model for the Galactic structure, and marginally on the choice of the extinction law, which is necessary to derive the opacity from the optical depth along the line of sight (see equation 24 in Drimmel & Spergel 2001). Thus, the map does not allow us to obtain a new determination of the Cepheids' distances *independent* of the extinction law.[2]

The values of A_{K_S} obtained from the dust map as a function of the true distance modulus is shown as a thick solid line in Fig. 3 for the five line of sights where the Cepheids are located (same colours as in Fig. 1). The lines $\mu_{K_S} = $ constant for each Cepheid are indicated by the dashed lines in Fig. 3, and their intersections with the solid lines of the corresponding colours, highlighted by the stars, determine the true distance modulus obtained on the basis of the extinction map (see Table 3). In Fig. 3, we also show the distances derived on the basis of the H-, K_S-band PL relations, and assuming the C89 (empty circles) and the N06 (empty squares) coefficients, together with the associated errors, indicated by the grey error bars. Note that

[2]However, Drimmel et al. (2003) adopted the extinction law by Rieke & Lebofsky (1985) and internally validated their choice by comparing the extinction predicted with the one measured for red-clump and OB stars in the inner and outer Galaxy. Here, we adopt the coefficient by C89, in order to extrapolate $A_{K_S} = 0.117 \times A_V$ in the IRSF photometric system, but the difference between the coefficients should be small (less than 1 per cent). This is necessary because Rieke & Lebofsky (1985) do not provide a general function for the extinction curve which could be extrapolated to different wavelengths, but they only provide $A_K = 0.112 \times A_V$.

the distance values can only change according to the dashed lines, and by assuming that the extinction law cannot be shallower then the C89 in the inner Galaxy, we consider the empty circles as the minimum possible distance for the five new Cepheids. Similarly, we cannot expect them to be any further of the distances indicated by the empty squares.

More specifically, the data plotted in this figure show that for Cepheids: ID-1, ID-4, and ID-5, the use of C89 reddening law provide values that are closer to the prediction from the dust map, and thus we adopt them as our best estimates. For Cepheids ID-2 and ID-3, instead, the N06 law gives values more consistent with what is predicted by the map, and we decided to take them as the best estimates for these Cepheids. The final adopted distances and their associated errors are given in the last column of Table 3. On the basis of these distances, and by assuming a J-band PL relation, we can also obtain the best estimate of the extinction coefficient A_{K_S}/A_J for each of the Cepheids, and we find that it is close to the C89 value (0.40) for two of them, while it attains slightly larger values than the one by N06 (0.33) for the others, thus confirming that the slope of the extinction law in this direction is likely in between the two.

The coloured triangles show the values of extinction and distances for new variables in the case they are Type 2 Cepheids. Also in this case, we assumed the PL relations by Bhardwaj et al. (2017) in the H and K_S bands calibrated to the LMC distance, and the coefficients first from C89 (triangles up) and N06 (triangles down). The values of distances and extinction obtained are inconsistent

Table 1. Coordinates and photometric data of the newly discovered Cepheids.

Name	RA (h:m:s)	Dec. (d:m:s)	Period (d)	$\langle J \rangle_F^a$ (mag)	$\langle H \rangle_F^a$ (mag)	$\langle K_S \rangle_F^a$ (mag)	$\langle J \rangle_T^b [\chi^2]^c$ (mag)	$\langle H \rangle_T^b [\chi^2]^c$ (mag)	$\langle K_S \rangle_T^b [\chi^2]^c$ (mag)
ID-1 [purple]	15:05:56.07	−58:10:43.5	9.036	11.934 ± 0.003	10.606 ± 0.003	10.017 ± 0.003	11.936 ± 0.005 [16]	10.608 ± 0.005 [11]	10.021 ± 0.006 [10]
ID-2 [orange]	15:06:00.57	−58:27:43.4	10.260	13.973 ± 0.005	12.030 ± 0.003	11.008 ± 0.003	13.977 ± 0.009 [8]	12.030 ± 0.005 [8]	11.010 ± 0.005 [15]
ID-3 [magenta]	15:06:34.68	−58:23:58.1	9.996	14.042 ± 0.004	11.940 ± 0.003	10.878 ± 0.003	14.054 ± 0.008 [14]	11.939 ± 0.005 [9]	10.880 ± 0.005 [6]
ID-4 [cyan]	15:07:01.83	−58:16:56.1	6.644	10.882 ± 0.001	9.689 ± 0.002	9.173 ± 0.003	10.887 ± 0.003 [25]	9.692 ± 0.004 [18]	9.175 ± 0.005 [10]
ID-5 [lime]	15:07:57.59	−58:25:35.8	4.407	13.972 ± 0.004	12.318 ± 0.002	11.535 ± 0.003	13.972 ± 0.007 [17]	12.322 ± 0.005 [14]	11.536 ± 0.005 [15]

[a] Mean magnitudes obtained on the basis of the Fourier fit.
[b] Mean magnitudes obtained on the basis of the template fit.
[c] Chi-squared of the best-fitting template.

Table 2. Fourier parameters for the *J*-band light curves of the new Cepheids.

Name	A_1 (mag)	R_{21}	R_{31}	Φ_{21} π	Φ_{31} π
ID-1	0.113	0.276	0.092	1.26	0.02
ID-2	0.091	0.349	0.404	1.45	0.88
ID-3	0.133	0.112	0.087	1.74	1.67
ID-4	0.140	0.321	0.153	1.25	−0.01
ID-5	0.065	0.528	0.237	1.04	1.47

with the absorption along the line of sight as predicted by the dust map. Thus, this hypothesis can be discarded. However, Cepheids ID-4 and ID-5 have short periods, thus they could be classical Cepheids but pulsating in the first overtone. In this case, they would be intrinsically brighter of ∼0.5 mag (see e.g. Feast & Whitelock 1997; Kovtyukh et al. 2016), and therefore ∼1 kpc further. However, first-overtone pulsators are characterized by a different range of Fourier parameters and by smooth sinusoidal light curves, without the bumps clearly visible on the rising branch of the light curves in Fig. 1.

3.2 The position of the new Cepheids in the Galactic disc

The position of the new Cepheids, projected on to the Galactic plane is shown in Fig. 4. We used a cylindrical coordinate system (x, y, z) centred on the Sun position, which is located at a distance from the Galactic Centre: $R_\odot = 7.94 \pm 0.37 \pm 0.26$ kpc (Groenewegen, Udalski & Bono 2008; Matsunaga et al. 2013, and references therein). We also show the position of all the known Galactic Cepheids for which homogenous metallicity were estimated by our group[3] (grey diamonds; Genovali et al. 2014, hereinafter G14), by Martin et al. (2015, blue squares), and by Andrievsky et al. (2016, ASAS181024–2049.6, blue diamond). Filled symbols indicate all the objects in the ID, defined as the region within 2.5 and 8 kpc from the Galactic Centre *and* within 250 pc from the Galactic plane. Note that we do not include here the Cepheids found beyond the Galactic Centre by Matsunaga et al. (2016); Dékány et al. (2015a,b) as there are no spectroscopic observations for them available in the literature, thus they are not relevant for the present discussion.

In order to investigate possible correlations between the new Cepheids' position and the spiral arms of our Galaxy, we also plot their distribution according to Reid et al. (2016), including the Scutum (dark-cyan line), the Sagittarius (violet line), and the Perseus (indigo line) arms. We also show the expected location of the Norma arm according to a 4-arm logarithmic spiral model in red, but the exact morphology of the spiral arms in the fourth Galactic quadrant is still very uncertain (Vallée 2017). The position of the Red Supergiant clusters RSC1 and RSC2 discovered by Davies et al. (2009b) is also shown, since they are located at similar galactocentric distances with respect to the new Cepheids, but at positive *l*, therefore close to the edge of the Galactic bar. Finally, the position of 5 young (≲100 Myr, Spina et al. 2017, magenta diamonds) and 12 intermediate-age (≳100 Myr, Jacobson et al. 2016, dark-cyan diamonds) Open Clusters (OCs) investigated by the *Gaia*-ESO survey is also shown for comparison.

By using the period–age relation determined by Bono et al. (2005), we can determine the individual ages of the new Cepheids

---

[3] We removed BC Aql from the sample, because a recent improved coverage of its optical light curve indicates it is a Type 2 Cepheid (see the AAVSO website at http://www.aavso.org/vsx/ for more details).
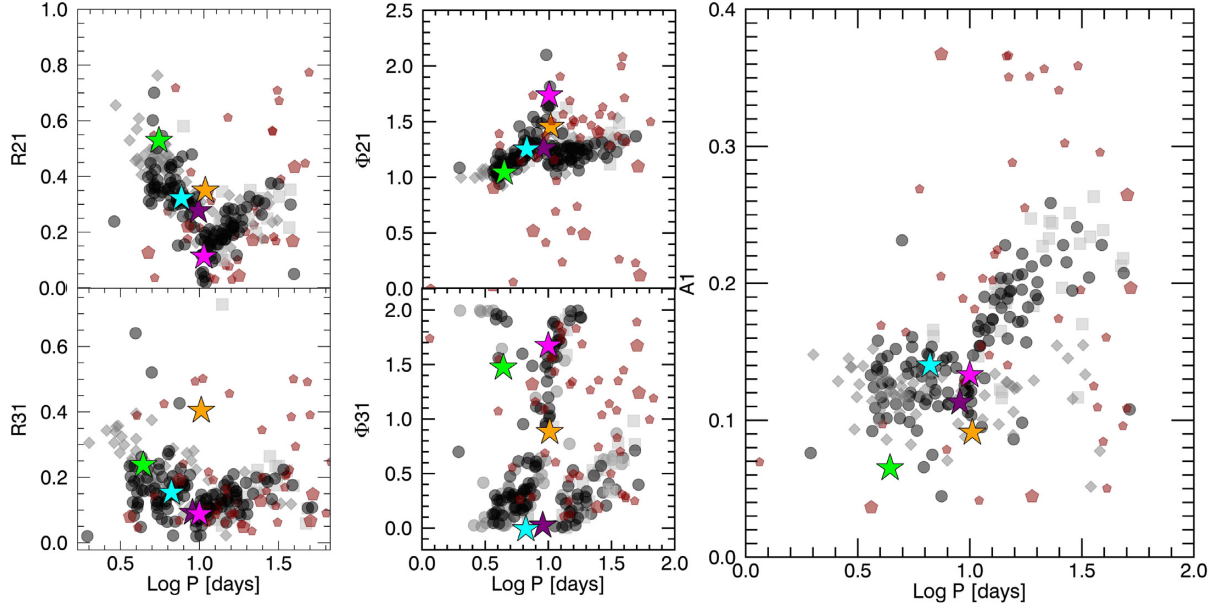
Figure 2. Fourier parameters of *J*-band light curves for the newly discovered Cepheids (same colours as in Fig. 1) compared to the parameters of known classical Cepheids in the MW (Laney & Stobie 1992; Monson & Pierce 2011, dark dots), in the Large (Persson et al. 2004, grey squares) and in the Small (Inno et al. 2015, grey diamonds) Magellanic Clouds. We also include data for Type 2 Cepheids in the MW (Matsunaga et al. 2013, large red pentagons) and in the Large Magellanic Cloud (Bhardwaj et al. 2017, small red pentagons). This comparison shows that the Fourier parameters of the new Cepheids are compatible with the ones of classical Cepheids. However, the overlap between the Fourier parameters of classical and Type 2 Cepheids does not allow for a conclusive distinction between them on the basis of these parameters alone. Therefore, we rely on the discussion on their distance and extinctions in Section 3.1 to further validate our classification.

Table 3. Distances and extinction of the newly discovered Cepheids.

Name	$\mu_{0,C89}{}^a$ (mag)	$A_{K_S,C89}{}^a$ (mag)	$\mu_{0,N06}{}^b$ (mag)	$A_{K_S,N06}{}^b$ (mag)	$\mu_{0,B16}{}^c$ (mag)	$A_{K_S,B16}{}^c$ (mag)	Distance^d (kpc)	$A_{K_S}/A_J{}^e$
ID-1	14.52 ± 0.06	0.98	14.73 ± 0.05	0.77	14.48	1.0	$7.9^{+0.8}_{-0.2}$	0.41
ID-2	14.93 ± 0.06	1.76	15.31 ± 0.05	1.38	15.27	1.5	$11.5^{+0.3}_{-1.9}$	0.36
ID-3	14.68 ± 0.06	1.84	15.07 ± 0.05	1.45	15.01	1.5	$10.5^{+0.3}_{-1.8}$	0.36
ID-4	13.42 ± 0.06	0.83	13.59 ± 0.15	0.65	13.45	0.8	$4.8^{+0.5}_{-0.1}$	0.37
ID-5	14.67 ± 0.06	1.35	14.95 ± 0.15	1.06	14.63	1.4	$8.7^{+1.3}_{-0.2}$	0.40

^{a}Based on the extinction law by Cardelli et al. (1989) and *H*-, K_S-band PL relations.
^{b}Based on the extinction law by Nishiyama et al. (2006) and *H*-, K_S-band PL relations.
^{c}Based on the dust map by Bovy et al. (2016) and K_S-band PL relation.
^{d}The best distance estimates according to data shown in Fig. 3 with the associated total (random and systematic) uncertainty.
^{e}Extinction coefficients determined on the basis of our best distances.

and we found that three of them have ages of about 45 Myr, while ID-4 and ID-5 are about 20 Myr older. Thus, only the young OCs and the RSCs have ages comparable to the ones of the Cepheids.

4 THE SPECTROSCOPIC DATA SET

During the semester 2013 March–September, we collected NIR spectra with ISAAC at VLT for all the new Cepheids discovered in the ID and for the Cepheid V367 Sct, which we adopt as a calibrating Cepheid to compare metallicity abundances based on NIR spectroscopy with the one derived from optical spectra. We adopted the medium-resolution ($R \sim 3100$) spectroscopic (SWS1_MR) grism with the central wavelength $\lambda = 1.185$ μm.

We have retrieved the raw files from the ESO Science Archive Facility, using the CalSelector option to associate the appropriate calibration files to the science ones. Due to the ABBA observing strategy, the sky subtraction has been done in the usual A-B/B-A

way. Spectra extraction on the single frame has been accomplished using *apall*. The extracted spectra were then normalized via the *continuum step* in IRAF. The wavelength solution has been directly derived from the telluric standards, using as a primary reference a template absorption spectrum obtained from the ESO software SKYCALC.[4] The target spectra were then cross-correlated with the wavelength calibrated telluric (in pixels) and shifted accordingly. This allows both the telluric correction and wavelength calibration of the targets. The reduced spectra were then corrected for atmospheric absorption features by adopting MOLECFIT, which is a software developed by the Institute for Astro- and Particle Physics at the University of Innsbruck for ESO. This tool is based on synthetic transmission spectra which can then be directly fitted to the ob-

---

[4]http://www.eso.org/observing/etc/bin/gen/form?INS.MODE=swspectr + INS.NAME = SKYCALC
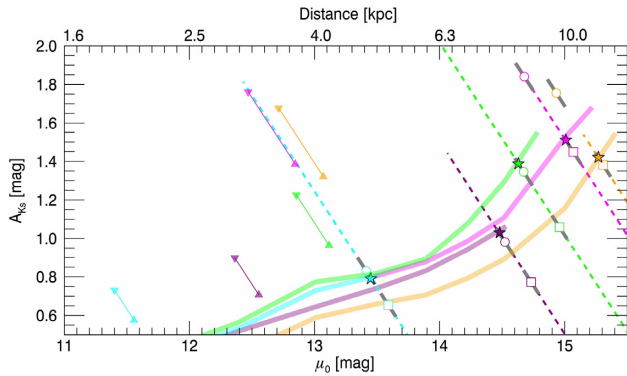
Figure 3. Absorption in the K_S band as a function of the true distance modulus from the *mwdust* map (Bovy et al. 2016) for the five new Cepheids (solid lines, ID-1: purple, ID-2: light red; ID-3: magenta, ID-4: cyan, ID-5: lime). The dashed lines are lines of constant μ_K, and their intersections with the solid lines, which are indicated by the stars, provide the estimate of the Cepheids' distances on the basis of the dust map. The empty circles indicate the distances obtained by using the C89 extinction coefficients, while the empty squares are the distances based on N06. These values indicate the minimum and maximum values that the Cepheids' distances can attain. Finally, the triangles show distances and extinction obtained by assuming that the new variables are Type 2 Cepheids, by adopting the C89 (triangles up) or the N06 (triangles down) reddening law. These values are clearly inconsistent with the predicted absorption along the line of sight, thus further confirming our classification as classical Cepheids.

served spectra. Finally, the spectral analysis has been performed by adopting a novel technique we recently developed, and applied for the first time to blue supergiants in the LMC (Urbaneja et al. 2017). This technique is based on existing precomputed grids of synthetic LTE spectra based on the MARCS models. The grid spans a range of effective temperature $T_{\rm eff}$ between 4000 and 7000 K with a spacing of 250 K, and a range of surface gravity $\log g$ up to 3.5 dex, with a step of 0.25 dex, with a solar-scaled chemical composition for metallicities [Fe/H] from -0.75 to $+0.75$ dex, with again a step of 0.25 dex. On top of the MARCS grid, we also compute models with TURBOSPECTRUM for improving the sampling in micro-turbolence. In fact, the MARCS models are only provided with a microturbolence of 2 and 5 km s^{-1}. By using TURBOSPECTRUM, we are able to also sample intermediate and larger values, up to 8 km s^{-1}. The stellar parameters and abundances are then obtained by a best fitting of the synthetic to the observed spectra, for the four parameters ([Fe/H], $T_{\rm eff}$, $\log g$, v_t) derived simultaneously, with the fit performed through a sophisticated automated procedure based on Monte Carlo Markov Chain techniques. For each parameter, this procedure allows us to recover a probability distribution, and the final value is chosen as the centre of that distribution, while the associated uncertainty corresponds to the first and third quartile of the distribution.

The spectra reduced and corrected for the telluric lines are shown in Fig. 5 together with the identification of some of the lines used for the metallicity estimate, while the physical parameters measured are listed in Table 4. In our technique, we only use specific wavelengths windows (marked thicker in Fig. 5) for performing the fit. For instance, all the carbon lines (C I) are excluded because carbon can be affected by stellar evolution processes. Note that in the case of ID-1 and ID-4, we had two independent observations at two different pulsation phases, so we adopted the mean of the metallicity obtained from the two spectra, weighted for their SNR.

Some of the metal lines identified and used for performing the fit with the synthetic models are labelled in Fig. 5. Note that there are also several intense DIBs (diffuse interstellar bands) present in the spectra of the new highly obscured Cepheids, which are not visible in the spectrum of the calibrator V367 Sct. Excluding the most prominent one at 1.18 (Joblin et al. 1990), that is already known, the other DIBs are rarely observed, because the line-of-sight extinction is not high enough. This is the case of the structures centred around 1.17 μm and the one at 1.20 μm. The equivalent width (EW) of these lines carries information on the extinction towards the Cepheids, but a quantitative determination is not possible yet, because an empirical relation between the EW of these lines and the corresponding colour excess has not been calibrated yet. However, the fact that the measured EW are larger for Cepheids ID-2 and ID-3 ($\sim$900 mÅ) and smaller for Cepheid ID-4 ($\sim$500 mÅ), further supports the current determination of their distances and extinction.

4.1 Consistent metallicities between optical and NIR analyses

Cepheids have been widely adopted to investigate the Galactic disc radial metallicity gradient, by our group (Lemasle et al. 2007, 2008; Pedicelli et al. 2010; Genovali et al. 2014; da Silva et al. 2016) and in the literature (Yong et al. 2006; Sziládi et al. 2007; Luck et al. 2011; Luck & Lambert 2011; Martin et al. 2015; Andrievsky et al. 2016). However, all these investigations rely on high-resolution *optical* spectra, and therefore they are limited to bright and/or nearby Cepheids, while the metallicity gradient is mostly influenced by Cepheids located in the inner and outer regions of the disc. Because of the high amount of extinction, NIR spectroscopy is necessary to investigate the metallicity gradient in such critical regions. Unfortunately, while the method to determine the stellar parameters from optical spectra is very well known and tested, NIR spectroscopy is still in its infancy and, in fact, this is *the very first study in which Cepheids' parameters and chemical abundances are obtained from NIR-medium-resolution spectra.*

Thus, we first need to ensure the compatibility of our results with the ones obtained by using the *standard* approach as in Genovali et al. (2014, and references therein) To this purpose, we tested the metallicity abundances obtained from the ISAAC spectra of the calibrating Cepheid V367 Sct against the ones obtained from four optical spectra collected at different epochs. Genovali et al. (2014) analysed these spectra and found a mean abundance [Fe/H] $= 0.04 \pm 0.08$ dex, where the error is given by the rms of the different measurements, and the typical uncertainty on individual determinations ranges from 0.13 to 0.18 dex. The individual estimates as a function of the pulsation phase are shown in the top panel of Fig. 6. The mean value is indicated by the solid blue line, while the dashed lines show the rms around the mean. On the basis of the ISAAC spectrum, we find [Fe/H] $= -0.11 \pm 0.15$ dex (red dot in the top panel of Fig. 6), which agrees within 1σ with the results from the optical data, based on the EW method.

To further confirm the consistency of our NIR analysis, we also compare the effective temperature obtained from optical and NIR spectra of V367 Sct at the different observed phases. The middle panel of Fig. 6 shows the light curve in the V band from ASAS.[5] V367 Sct is a double-mode Cepheid, folded at its fundamental period of 6.29307 d, therefore the large scatter in the photometric data.

---

[5] http://www.astrouw.edu.pl/asas/?page = acvs
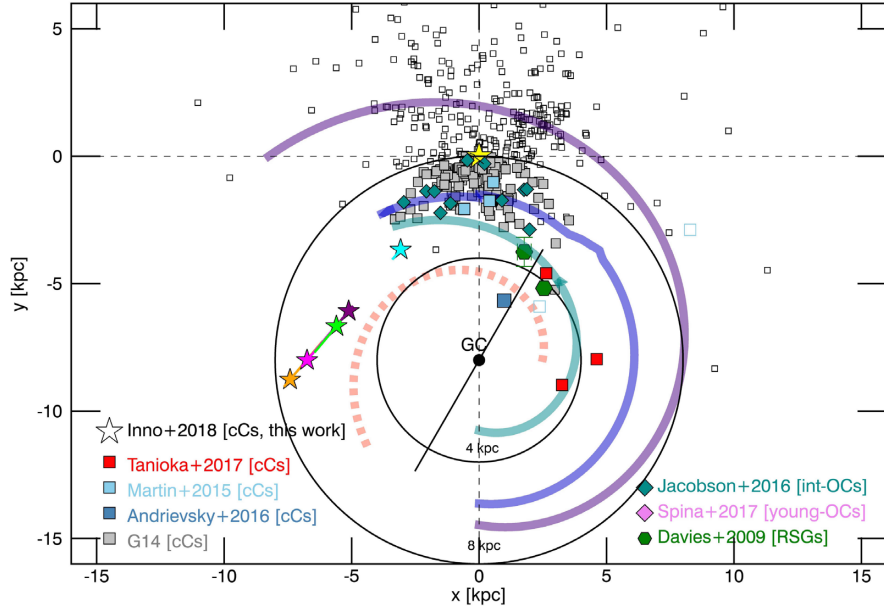
Figure 4. Position of the newly discovered Cepheids projected on to the Galactic plane (ID-1: purple, ID-2: light red; ID-3: magenta, ID-4: cyan, ID-5: lime). The squares show the position of currently known Galactic Cepheids (Tanioka et al. 2017; Andrievsky et al. 2016; Martin et al. 2015; Genovali et al. 2014) while the blue rhombs indicate young and intermediate-age Open Clusters for which accurate abundances and positions have been provided by the *Gaia*-ESO Survey (Jacobson et al. 2016; Spina et al. 2017). The green hexagons shows the position of the two red supergiants clusters (RSGC1 and RSGC2) presented in Davies et al. (2009b). Filled symbols indicate all objects located within 8 kpc from the Galactic Centre and inside 250 pc above and below the Galactic Plane. The spiral-arm pattern of our Galaxy as recently revised by Reid et al. (2016) is also over plotted: the Scutum arm (dark cyan), the Sagittarius arm (blue), the Perseus arm (indigo), and the Norma arm (red). The black lines show circles at galactocentric radius of $R_{GC} = 4$ kpc and of $R_{GC} = 8$ kpc. The position of the Sun (yellow dot) of the Galactic Centre (black dot) and the central long bar according to Bland-Hawthorn & Gerhard (2016) are also shown.

We performed a Fourier fitting of the light curve and mirrored it in order to qualitatively predict the shape of the temperature curve over the Cepheid pulsation cycle. In particular, we normalized the curve, multiplied it for the expected temperature variation of a Cepheid along the pulsation cycle ($\sim$1000 K) and added the mean values of the temperature as determined from the spectra ($\sim$6400 K). The new curve is plotted in the middle panel, where also the effective temperature measured on the optical (collected with UVES: blue dots; collected with FEROS: cyan dots) spectra (Genovali et al. 2014; Proxauf 2017) and on the ISAAC spectrum (red dot) are shown.

This figure shows that the difference in temperature found in the optical and in the NIR regime are consistent within the expected change in temperature due to the pulsation mechanism. All the values adopted for V367 Sct are listed in Table 5.

4.2 Cepheids' centre-of-mass velocity from single-epoch spectroscopic data

By comparing the observed to the synthetic spectra in the model grid we obtained the instantaneous radial velocities of the Cepheids, which includes the barycentric velocity of the star (the so-called γ-velocity) and the pulsation velocity projected along the line of sight. Thus, we need to correct the observed velocity for the pulsation velocity at the observed phase. To this purpose, we computed new radial-velocity templates which allow us to perform such correction (e.g. see also: Inno et al. 2015; Matsunaga et al. 2015). We constructed velocity curve templates for Galactic Cepheids with period similar to the new ones, and in particular for the two period ranges: $4 \lesssim P \lesssim 7$ (template-1) and $9 \lesssim P \lesssim 10.5$ (template-2). Thus, we

adopted the K_S-band light curves and the radial velocities curves of 20 (template-1) and 8 (template-2) nearby Cepheids, compiled by Storm et al. (2011a), to calibrate such templates as described in the following.

We fitted a seventh-order Fourier series to both the light and radial-velocity curves, and computed the peak-to-peak amplitude of the fit. As shown in Fig. 7, the amplitude in the K_S band, Δ_{K_S}, is tightly correlated with the velocity amplitude, Δ_{RV}, and we calibrated the relations:

$$\Delta_{RV}/\Delta_{K_S} = 160 \pm 2.95 \, \text{km s}^{-1}\text{mag}^{-1}, \, [\text{template-1}]$$
$$\Delta_{RV}/\Delta_{K_S} = 180 \pm 4.19 \, \text{km s}^{-1}\text{mag}^{-1}, \, [\text{template-2}] \qquad (3)$$

which allow us to predict Δ_{RV} from the Δ_{K_S} of the new Cepheids. Note that the quoted error is the dispersion around the mean Δ_{RV}/Δ_{K_S} relation. In the case of the new Cepheids ID-1 and ID-4, we collected ISAAC spectra at two different pulsation phases, and the measured velocities are shown in Fig. 8 together with the radial-velocity template adopted (template-2 for ID-1, top panel; template-1 for ID-4, bottom panel). The final γ-velocities obtained are indicated by the dashed line, while the shadowed area delimitates the error interval. In fact, the uncertainty on the final estimate is given by the sum in quadrature of the error on the measurement of the Doppler velocity (1 kms^{-1}), the dispersion given in equation (3), and the scatter around the templates rescaled by the amplitude ($\sim$0.1 × Δ_{RV} km s^{-1}).

Within the period ranges we selected, the Cepheids show very similar variations in light and velocity, and we can use the templates described above to predict the pulsation amplitude for all the new Cepheids. The resulting γ-velocities in the local standard of rest (LSR), V_{LSR}, are listed in Table 4 and shown in
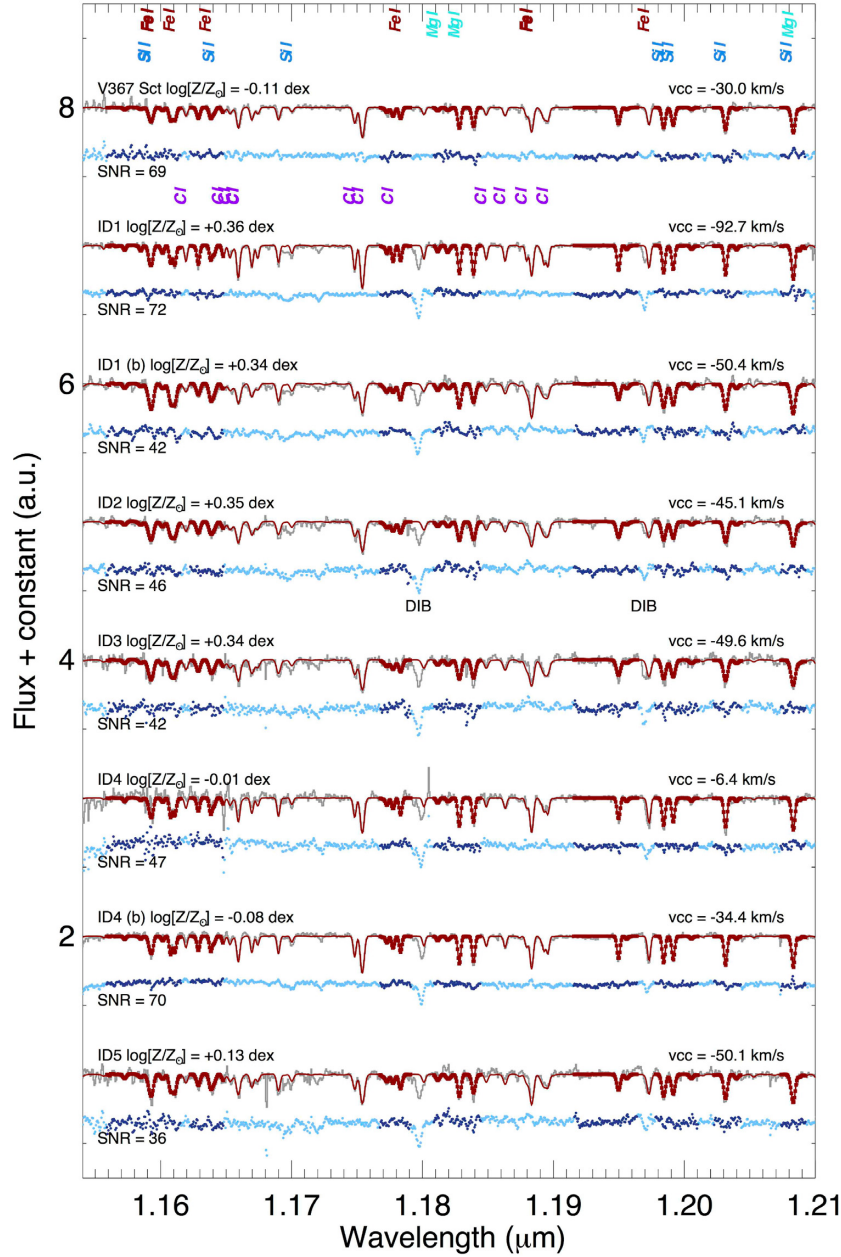
Figure 5. The analysed ISAAC spectra for the different targets. The grey lines show the observed spectra, while the red line shows the best-fitting model, and the blue lines in the bottom indicate the residuals. Note that we did not fit the full regime but only the windows indicated by the thick lines. Some of the identified lines used for the fits are labelled on the top of the first spectrum (mainly Fe I, Si I, and Mg I), while the C I lines excluded are labelled on top of the second one. Moreover, we also identify a DIB at 11 797 Å (Joblin et al. 1990; Hamano et al. 2016) and three more at 11 697, 11 721, and 11 969 Å, which are only present in the spectra of the newly discovered Cepheids. The SNR and the Doppler velocity of each spectrum is also given in the label.

Fig. 9. The complete set of radial-velocity templates for classical Cepheids will be given in a forthcoming paper (Inno et al. in preparation).

5 THE KINEMATICS OF YOUNG STARS IN THE INNER GALAXY

We compared the kinematics of the new Cepheids with the one predicted by adopting the rotation curve empirically calibrated by Reid et al. (2009), which assumes a solar distance $R_\odot = 8.0$ kpc, and a circular velocity of the Sun $\Theta_\odot = 240$ kms^{-1} (solid thick line).

Fig. 9 shows the expected velocity as a function of the distance d from us, together with the measured V_{LSR} of the new Cepheids. Only ID-1, ID-5, and marginally ID-3 show a kinematics consistent with the disc rotation, while the others show significant differences. This difference between the observed V_{LSR} and the one predicted by a flat rotation curve at the same location is indicated as a *velocity drift* hereinafter. Negative velocity differences at positive longitudes imply a faster rotation, while they correspond to a slower rotation at negative longitudes. Therefore, we compute the absolute difference between the observed radial velocity along the line of sight and the one predicted on the basis of the pure circular rotation, and then we associate to it a positive sign at negative longitudes, and
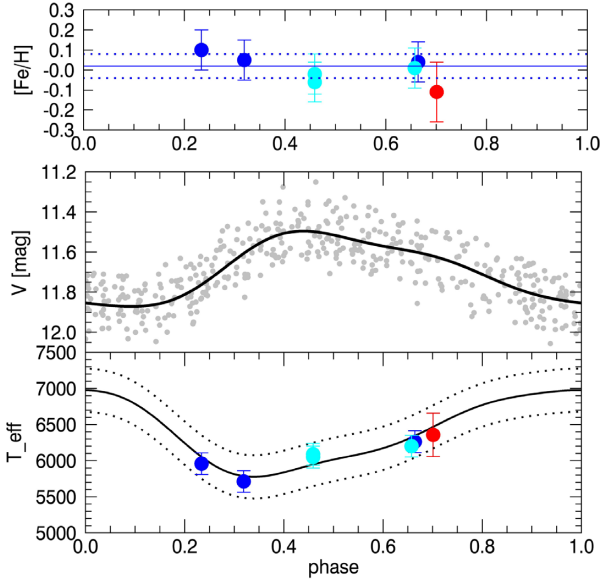
Figure 6. Comparison of the calibrator Cepheid metallicity and effective Temperature from optical and NIR spectra. *Top*: Iron abundances obtained from the optical (UVES, blue dots; FEROS, cyan dots) and the NIR (ISAAC, red dot) spectra as a function of the pulsation phase at the time of observation. The blue solid line shows the mean value found on the basis of the optical data, while the dashed lines indicate the rms. The value obtained with our analysis for the NIR spectrum is consistent within 1σ with the ones in the literature. *Middle*: Light curve in the V band for the calibrating double-mode Cepheid V367 Sct from ASAS and the Fourier fit to it. *Bottom*: Effective temperature obtained from the optical UVES (blue dots) and FEROS (cyan dots) spectra compared to the one obtained with ISAAC (red dot). The solid line is the mirrored light curve which is used to trace the variation of the effective temperature due to the pulsation cycle, while the dashed lines indicated the expected rms. The effective temperature obtained by our new spectral analysis technique is in excellent agreement with the ones obtained by using a completely different approach (see e.g. Kovtyukh et al. 2010) and wavelength regime (optical).
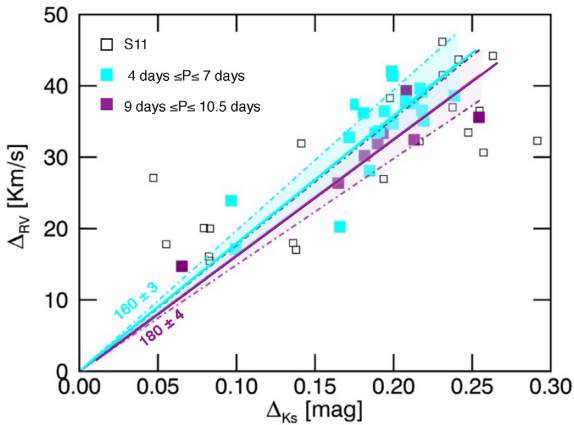
Figure 7. The velocity amplitude, Δ_{RV}, as a function of the luminosity amplitude in the K_S band, Δ_{K_S}, for the Cepheids in Storm et al. (2011a) that we used to calibrate our templates. The cyan squares indicate the Cepheids in the period range of template-1, while the purple indicate the ones in the range of template-2. The best-fitting linear relation that we obtained is also indicated by the solid line in the corresponding colour. The shadowed area indicate the standard deviation around the relation, which we considered as the error associated with the slope in equation (3).
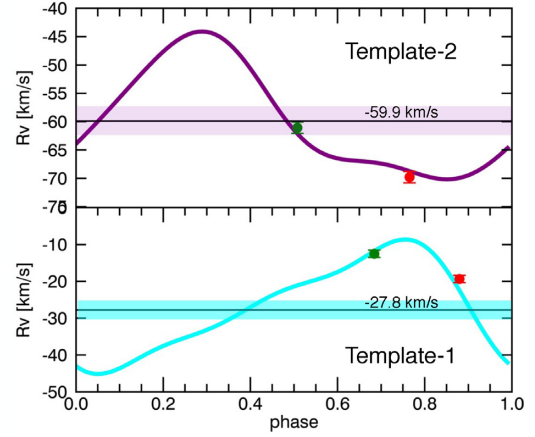
Figure 8. Radial-velocity templates applied to the new Cepheids ID-1 (top panel, purple solid line: template-2, periods ranging from 9 to 10.5 d) and ID-4 (bottom panel, cyan solid line: template-1, periods ranging from 4 to 7 d) for which spectroscopic observations at two different phases were available. The dots show the observed heliocentric velocity of the new Cepheids at the phase of the first (red) and second (green) observations (see Table 3). The solid black lines give the resulting mean radial velocity, which corresponds to the γ-velocity of the Cepheids, while the shadowed area delimitate the ± 5 km s^{-1} uncertainty.
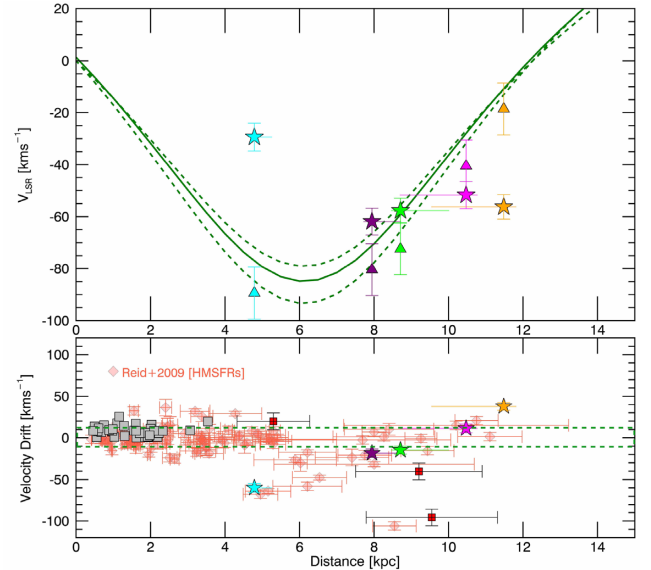
Figure 9. *Top*: Line-of-sight velocity of the new Cepheids with respect to the LSR (coloured star marks) as a function of distance, compared to velocity predicted according to the Galactic rotation curve of Reid et al. (2014, solid green line). The dashed lines indicate a variation of ± 10 km s^{-1} for the circular velocity of the Sun: $V_{\odot} = 240$ km s^{-1}. Only two (ID-1, purple and ID-5, lime) out of the five new objects seem to have velocity consistent with the expected rotation, while the other three are either rotating slower (ID-4, cyan) or faster than expected. The coloured triangles indicate the expected V_{LSR} of the gas on the basis of the dynamical simulation by Sormani et al. (2018) and are similar to those predicted from the circular rotation curve. *Bottom*: Velocity drifts of the new Cepheids as a function of distance, compared to the ones of Cepheids in G14 with measured γ velocity by Storm et al. (2011a, grey squares), three Cepheids from Tanioka et al. (2017, red squares), and the HMSFRs by Reid et al. (2014). The green dashed lines indicate again the difference of ± 10 km s^{-1} from the predicted velocity. The new Cepheids have velocity drifts which seem to be proportional to the distance, thus indicating a systematically different velocity pattern. The HMSFRs at similar distances seem to follow a similar trend.

Table 4. Physical parameters, iron abundances, and kinematics of the newly discovered Cepheids.

Name	Epoch MJD	ϕ^J_{max}	SNR	T_{eff} ± 300 (K)	$\log g$ ± 0.25 (dex)	v_t ± 1.0 (km s^{-1})	[Fe/H] ± 0.15 (dex)	R_G (kpc)	V_{obs}[a] (km s^{-1})	V_{LSR}[b] (km s^{-1})	V_{gas}[c] (km s^{-1})
ID-1	6527.484	0.77	72	6738	2.12	6.4	0.36	$5.5 \pm^{+0.3}_{-0.1}$	-70 ± 1	-60 ± 5	-80 ± 10
ID-1	6407.688	0.51	42	6000	1.88	5.6	0.34	$5.5 \pm^{+0.3}_{-0.1}$	-61 ± 1	-60 ± 5	-80 ± 10
ID-2	6407.723	0.51	46	6290	1.64	5.2	0.35	$7.5 \pm^{+0.2}_{-1.3}$	-56 ± 1	-52 ± 5	-19 ± 10
ID-3	6407.773	0.83	42	6227	1.64	5.2	0.34	$6.8 \pm^{+0.2}_{-1.0}$	-60 ± 1	-50 ± 5	-41 ± 10
ID-4	6401.898	0.88	47	6176	2.12	6.8	-0.01	$5.3 \pm^{+0.1}_{-0.1}$	-19 ± 1	-27 ± 5	-89 ± 10
ID-4	6533.484	0.68	70	6210	1.64	5.6	-0.08	$5.3 \pm^{+0.1}_{-0.1}$	-13 ± 1	-27 ± 5	-89 ± 10
ID-5	6407.832	0.26	36	6018	1.87	5.0	0.23	$5.8 \pm^{+0.7}_{-0.10}$	-61 ± 1	-56 ± 5	-72 ± 10

[a]Heliocentric observed radial velocity.
[b]γ-velocity respect to the LSR.
[c]Velocity for gas particles at the Cepheids' location in the simulation by Sormani et al. (2018).

Table 5. Physical parameters and iron abundances of the calibrator Cepheid: V367 Sct.

Epoch MJD	ϕ^J_{max}	SNR	T_{eff}	$\log g$	v_t (km s^{-1})	[Fe/H] (dex)	Instrument	Resolution
6405.0	0.70	100	6358 ± 300	1.9	6.3	-0.11 ± 0.15	ISAAC	3000[a]
6175.1	0.24	100	5959 ± 84	1.2	4.2	0.10 ± 0.10	UVES	38 000[b]
4709.6	0.32	98	5712 ± 93	1.3	3.4	0.05 ± 0.10	UVES	38 000[b]
6184.0	0.67	98	6262 ± 196	1.0	3.4	0.04 ± 0.10	UVES	38 000[b]
3156.8	0.46	150	6089 ± 107	2.0	4.9	-0.06 ± 0.10	FEROS	48 000[b]
3156.9	0.46	151	6111 ± 135	1.7	4.9	-0.02 ± 0.10	FEROS	48 000[c]
3157.8	0.66	146	6212 ± 150	1.8	3.8	0.01 ± 0.10	FEROS	48 000[c]

[a]This work.
[b]Spectra analysed in Genovali et al. (2014) and Proxauf (2017).
[c]Spectra analysed in Kovtyukh et al. (2016) and Proxauf (2017).

a negative sign for positive longitudes. As a result, a star with a positive velocity drift is moving faster than predicted from pure circular motion, while a star with a negative drift is moving slower. It is worth to mention that an error on the estimated distance for the new Cepheids would also produce artificial velocity drifts. However, the Cepheid ID-4 should be at least ∼2.5 kpc closer to us or ∼5.5 kpc farther in order to match the expected V_{LSR}, which would imply an error on the estimated distance larger than 3σ. This is quite unlikely, especially for this Cepheid, which is less obscured with respect to Cepheids ID-1 and ID-5, which have instead velocities consistent with the curve. Note that even in the case that the Cepheid ID-4 is pulsating in the first-overtone mode, the velocity difference would still be observed, as the star shall be located ∼1 kpc farther from us, where its expected velocity would be even larger.

Similarly, an error on the V_{LSR} would also produce the observed velocity drifts. The dominant source of uncertainty in the computed Cepheids' velocities is the correction for pulsation effects. However, it has been shown in the literature that Cepheids' pulsation velocity amplitudes are ∼5–30 km s^{-1} (Storm et al. 2011a,b), with possible modulations effects due to the rotation or presence of a companion ranging from several hundred ms^{-1} to a few kms^{-1} (Anderson 2016). The difference found here in the V_{LSR} is significantly larger (∼50 kms^{-1}). Once again, the velocity differences observed cannot be due to just measurements' errors. Moreover, we already found similar drifts for two Cepheids in the ID but located at positive Galactic longitudes (Tanioka et al. 2017) and concluded that either the Galactic rotation is slower in such regions, or the kinematics of the Cepheids is affected by the dynamical instabilities of the bar.

Here, we find that such drifts are proportional to the distance, and the disturbance caused by the presence of the bar cannot ac-

count for them. In order to check this, we used the simulations of Sormani et al. (2018), which model the gas flow in the MW barred potential and are able to reproduce the main observed characteristics of the atomic and molecular gas kinematics obtained through radio-frequency observations in the bar region ($l < |30|$ deg). These velocities are plotted as triangles of the same colours of the Cepheids to which they refer to, and they are very similar to the ones obtained on the basis of the purely circular rotation. Therefore, the dynamical influence of the bar is already small at the distances where the Cepheids are located.

The bottom panel of Fig. 9 shows the velocity drifts as a function of the heliocentric distance for the new Cepheids, the three Cepheids discussed in Tanioka et al. (2017), the Cepheids with velocity estimates in Storm et al. (2011a) and the high massive star-forming regions (HMSFRs) used by Reid et al. (2009) to determine the Galactic rotation located in the ID. The drifts systematically increase for increasing distance in the case of the new Cepheids, of two of the Tanioka et al. (2017) sample and of the HMSFRs at similar distances. This evidence indicates that such velocity pattern cannot be attributed to peculiar kinematics of the Cepheids, but must be related to a large-scale effect, such as e.g. the presence of the spiral-arms at these locations or of bar/spiral-arms interactions, as in the cases of external spiral galaxies (see e.g. Shetty et al. 2007; Beuther et al. 2017).

To explore at least qualitatively this scenario, we show in Fig. 10 the distribution of cold gas (left-hand panel) and young stars (age $\lesssim 0.3$ Gyr, right-hand panel) in the ID, simulated by Debattista et al. (2017, see their Section 4), and colour-coded by the deviation from the expected rotation velocity. While in the simulation by Sormani et al. (2018) the gas moves in an externally imposed
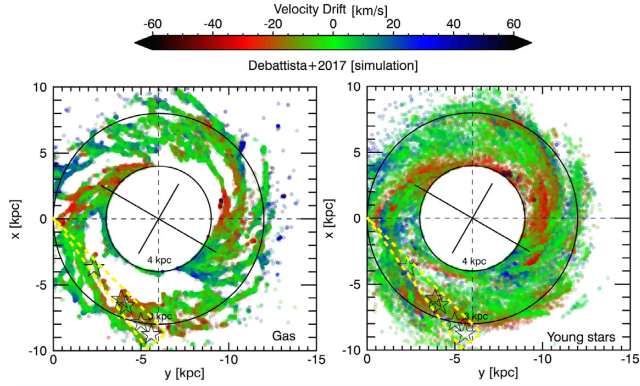
Figure 10. Deviation from circular orbits for gas (left-hand panel) and young stars (age $\lesssim$ 300 Myr, right-hand panel) in the simulation by Debattista et al. (2017). The central region ($R_{GC} \lesssim 4$ kpc) is masked as it is dominated by the presence of the bar, whose major and minor axes are also indicated. The colour map indicates the velocity drifts as indicated by the colourbar. Red stars are moving slower than expected, while blue stars are moving faster. The yellow lines indicate the region where the new Cepheids (black empty stars) would be located if the simulation would reproduce exactly the MW.

potential in which the only non-axisymmetric component is the bar, the simulation by Debattista et al. (2017) is self-consistent, with the potential obtained from a time-dependent *N*-body simulation in which spiral arms and other non-axisymmetric dynamical features are present in addition to the bar. Moreover, we rescaled the simulation in order to match the physical size and inclination of the MW central bar, and the rotation velocity at the Sun location (8 kpc) of 240 km s^{-1}. Thus, we computed the radial velocity V_{LSR} along the line of sight for each stellar particle in the simulated data, and then we subtracted from it the value predicted by using the rotation curve by Reid et al. (2009), as we did for the observed Cepheids. Moreover, we masked out the central region dominated by the bar. In fact, in the inner 4 kpc the deviation we computed has hardly a physical meaning, as the orbits are known to be not-circular due to the presence of the bar. Summarizing, the right-hand panel of Fig. 10 shows the position of stars that are moving either slower (red, negative drifts) or faster (blue, positive drifts) than expected. Such red and blue stars are not distributed uniformly in the plane, but they seem to trace the edges of spiral-arm-like features. This becomes even more evident by comparing their distribution to the one of the gas in the left-hand panel of the same figure. In fact, the gas seems to move systematically slower at the leading edges and faster at the trailing ones of these spiral-arm-like features, which is consistent with recent observational results (Hunt et al. 2017; Baba et al. 2018; Meidt et al. 2018). This behaviour is probably related to the spiral-arm resonances, which allow stars to spend enough time close to the arm itself, and to be initially decelerated by the local potential of the arm, and then accelerated when the arm has overtaken them. The presence of non-circular orbits of stars due to such resonances in the inner Galaxy has been indeed already suggested by Lépine et al. (2011) in order to explain the distribution and kinematics of molecular carbon monosulphides. The same resonance could be also responsible for the observed drifts of the new Cepheids, which have velocities consistent with the ones predicted by Lépine et al. (2011) for these non-circular orbits. Even though neither the available observed data or the simulated data allow us to completely characterize the orbits of the stars, it seems plausible that the drifts measured for the new Cepheids are produced by the
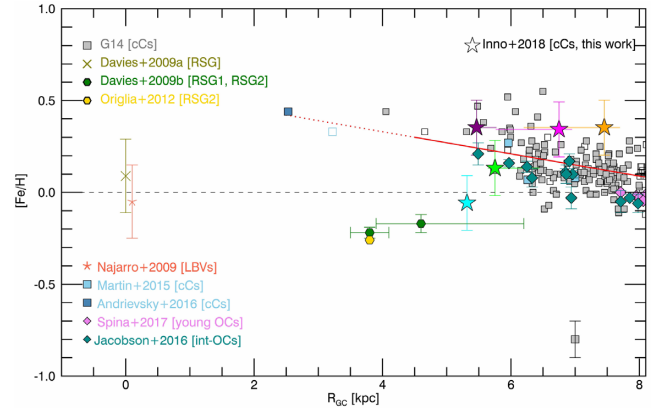
Figure 11. Iron abundances of the new Cepheids (coloured stars) versus their Galactocentric radius. The red line shows the metallicity gradient measured by G14 (solid line) and its extrapolation (dashed line) towards smaller galactocentric radii, which can be compared to the abundances of the Cepheids investigated by Martin et al. (2015) and Andrievsky et al. (2016). The hexagons mark the iron abundances of the two red supergiants clusters (RGSC1 and RGSC2) close to the bar's edge measured by Davies et al. (2009b, green) and by Origlia et al. (2013, yellow), while the olive cross shows the metallicity of the RGSC in the Galactic Centre (Davies et al. 2009a). The red asterisk with its error bar shows the metallicity range of LBVs in the Quintuplet cluster (Najarro et al. 2009). Finally, the violet diamonds show the metallicity of young (age $\lesssim$ 100 Myr) OCs measured by Spina et al. (2017), while the black triangle indicates the abundance for the calibrating Cepheid V367 Sct as estimated from the ISAAC spectrum.

presence of the same or similar resonances, and that the systematic trend shown in the bottom panel of Fig. 9 is related to the location of the stars across one or more spiral arms.
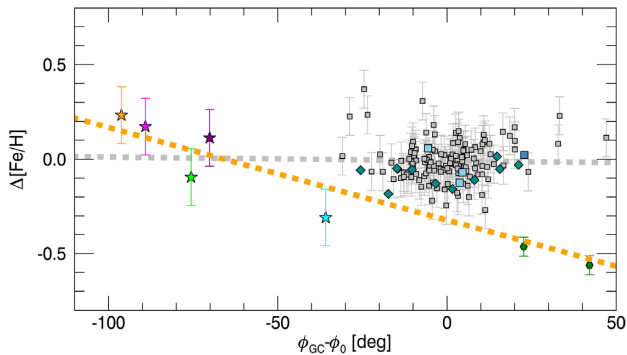
6 METALLICITY GRADIENTS IN THE INNER DISC

6.1 The radial gradient

In order to investigate the radial metallicity gradient in the ID, we plotted in Fig. 11 the iron abundances of the newly discovered Cepheids as a function of the Galactocentric radius compared to the abundances of all the other stellar tracers presented in Fig. 4: the two red supergiants clusters (RGSC1 and RGSC2), as measured by Davies et al. (2009b) and by Origlia et al. (2013). We also included the metallicity range covered by luminous blue variables (LBVs) in the Quintuplet cluster (Najarro et al. 2009). Note that all the iron abundances have been rescaled to the same solar abundance adopted in Section 4.

The iron content of the new Cepheids is on average compatible (within the error bars) with the one predicted by adopting a linear metallicity gradient on a wide range of Galactocentric distances $R_G \sim 4$–19 kpc, thus suggesting a homogenous chemical enrichment history, at least on the time-scale of Cepheids typical lifetime ($\sim$200 Myr).

However, one of the new Cepheids (ID-4) has solar metallicity, and contributes at increasing the dispersion around the linear metallicity gradient in the ID. In fact, given that the dispersion around the linear gradient reported in the literature is $\sigma([Fe/H])_{6.5 < R_{GC}/kpc \lesssim 13} \sim 0.09$ dex, the Cepheid ID-4 shows a 2σ discrepancy. This finding, together with the results for the RGSCs, indicates that the young stellar population in the inner part of the Galaxy cover a broad range of iron abundances: -0.3 dex

Figure 12. Residual with respect to the radial metallicity gradient as a function of the azimuthal angle about the Galactic Centre for the five new Cepheids and other stellar tracers in the ID from the literature (symbols are the same as in Fig. 11). We also show a linear fit to all the Cepheids' data, which is indicated by the grey dashed line, and it is consistent with a slope equal to zero (-0.000 ± 0.001). The orange dashed line shows the best fit to the metallicity residual restricted only to the new Cepheids and the RSGCs, with a slope of -0.0057 ± 0.0008, thus indicating a negative gradient.

$\lesssim$[Fe/H] $\lesssim$ 0.5 dex. A very similar metallicity range, i.e. -0.23 dex $\lesssim$ [Fe/H] $\lesssim 0.22$ dex, is also spanned by luminous cool stars within 30 pc of the Galactic Centre, as found by Cunha et al. (2007). Since the extrapolation of the linear metallicity gradient to $R_{GC} \sim 0$ would lead to significantly super-solar abundance in the Galactic Centre, a flattening of the ID gradient would be necessary to explain the metallicity composition of these stars. The metallicity content of the new Cepheids seems to suggest instead that the chemical composition of the inner part of the disc is characterized by a high degree of inhomogeneity.

6.2 The azimuthal gradient

In order to investigate if the metallicity inhomogeneity is related to a more complex spatial structure due e.g. to the presence of the bar, we compare the new Cepheids' iron content with the metallicity of the other Cepheids in the ID as a function of the azimuthal angle about the Galactic Centre. We performed this comparison following the argument by Davies et al. (2009b). They suggest that objects in the ID at negative *l* tend to have super-solar abundances, while metal-poor RSG clusters are located at positive *l*. They argue that this evidence is well justified by the inside-out infall scenario, when accounting for the dynamical effects due to the bar's instabilities, since the edge of the bar is towards positive Galactic longitudes (see Fig. 3). This would reflect into an azimuthal metallicity gradient in the ID.

We plot in Fig. 12 the residuals from the radial metallicity gradient of Cepheids as a function of their azimuthal angle, rotated of $\phi_0 = 30°$, i.e. the inclination angle of the bar respect to the *x*-axis.

If we consider the sample of Cepheids in the ID altogether, the data do not seem to support the presence of an azimuthal metallicity gradient, and indeed if we try to fit a linear relation, we find a slope consistent with zero (grey dashed line in Fig. 12). However, if we take into account only the newly discovered Cepheids and the RSGCs, we find a negative gradient significant at 7σ level. A possible explanation of this result is that the RSGCs and the new Cepheids belong to the same spiral arm, the Scutum arm, weather the other Cepheids belongs to (several) different arms overlapping along the same Galactocentric direction. However, arm–interarm metallicity variations are expected to be of the order of $\sim$0.02

dex (Bovy et al. 2014), thus quite smaller than the trend we find. Concluding, results based on Fig. 12 are difficult to interpret, as they are strongly biased by the incompleteness of the Cepheid sample. In order to obtain more quantitative and conclusive constraints on the metallicity distribution in the azimuthal directions, a more extensive sample of Galactic Cepheids with a well-defined selection function is needed.

7 CONCLUSIONS

We report the discovery of five Cepheids located in the fourth quadrant of the Galactic disc. These Cepheids are unique in that they allow us to probe the transition between the ID and the central regions of the Galaxy along the minor axis of the central bar, where they are expected to be less affected by its dynamical influences. We investigated the kinematics and iron abundance of the new Cepheids on the basis of NIR medium-resolution spectra collected with ISAAC@VLT. We built specific radial-velocity-curve templates in order to obtain the line-of-sight systemic velocity of the Cepheids from the observed radial velocity. We also performed a careful comparison between abundances determined on the basis of optical high-resolution spectra and NIR medium-resolution spectrum of the calibrating Cepheid V367 Sct. We found that the iron abundance estimates are consistent within the error bars, thus suggesting a negligible dependence on the wavelength regime and analysis techniques. Summarizing, we determined accurate distances, velocities and metallicities for the newly discovered Cepheids, even though they are located in highly obscured regions of the Galaxy.

In this paper, we show that the kinematics and the metallicity of these Cepheids are different from the ones of already known Galactic Cepheids in the ID. In fact (a) they move slower than expected if located at small galactocentric radii and faster if they are beyond the Galactic Centre; and (b) they are more metal rich at larger then at smaller azimuthal angles. However, given the little number of new Cepheids identified and the patchy, inhomogeneous selection function which characterizes the entire sample of known Cepheids in the MW, any interpretation of such findings must be taken with caution. None the less, our analysis show that the kinematics and metallicity content of young stars in the ID is strongly influenced by dynamical instabilities induced by the bar/spiral-arm-pattern.

We used the simulation by Sormani et al. (2018) to determine the motion of the gas at the location of the Cepheids. We found that the velocities predicted by the model are very similar to the ones predicted on the basis of the simple rotation curve within 10 km s^{-1}, which is the uncertainty associated with the model. We made the same comparison also for the three Cepheids presented in Tanioka et al. (2017), and we found similar results.

This indicates that the newly identified Cepheids are located too far with respect to the regions where the bar becomes dominant, thus bar-induced non-circular motions alone cannot account for the velocity drifts observed. However, such dynamical instabilities can be induced by any non-axisymmetric potential, also due e.g. to spiral arms, or even by bar/spiral-arm interactions. Recent results (e.g. Bobylev & Bajkova 2015; Baba et al. 2018) show that young stars have statistically significant velocity offset depending on their location either at the leading or trailing part of the spiral arm. Such velocity variations are expected to have amplitude of $\sim$6–10 km s^{-1} with respect to the Galactic rotation. These value are still two to three times smaller than the drifts we measured for the Cepheids in the ID, but they refer to the average perturbation, while the drifts can be larger for specific group of stars.

Summarizing, by comparing results from the simulations of Debattista et al. (2017) and Sormani et al. (2018) in Figs 9 and 10 we can conclude that (i) the bar cannot be the direct cause of the observed drifts; (ii) drifts with amplitudes of $\pm 60\,\mathrm{km\,s^{-1}}$ can be induced both in the gas and young stars by the presence of non-axisymmetric dynamical perturbations such as spiral arms outside the bar region ($R_{\mathrm{GC}} > 4\,\mathrm{kpc}$). Moreover, the simulation by Debattista et al. (2017) shows that stars at the leading edges of the spiral arms are mostly decelerated, while the ones at the trailing edges are accelerated, thus producing a systematic trend for velocity drifts across the arms. Finally, the observed deviations from the simple Galactic rotation also imply that the stars are moving in non-circular orbits, which are produced at dynamical resonances. Even though we cannot determine the new Cepheids orbits, it is plausible that they are moving in boxy-shaped orbits similar to the ones identified by Lépine et al. (2011) in the inner Galaxy.

The bar-like structure at the centre of the Galaxy is also a key ingredient for Galactic evolution models in order to explain the high star formation rate found in the Nuclear Bulge, since it is responsible for dragging gas and molecular clouds from the ID into the centre of the Galaxy (Athanassoula 1992; Kim et al. 2011). This scenario implies that the metallicity distribution of the ID should be similar to the one found in the nuclear bulge. Current findings show that the metallicity dispersion of the new Cepheids is indeed consistent with the metallicity of LBVs in the Quintuplet cluster by Najarro et al. (2009) and RSGCs in the Galactic Centre by Davies et al. (2009a). Moreover, recent measurements by Ryde & Schultheis (2015) for evolved stars in the nuclear bulge (M giants) also show a similar large metallicity range, i.e. -0.13 dex $\lesssim$ [Fe/H] $\lesssim 0.29$ dex, with a good overlap with the metallicity range covered by the new Cepheids, i.e. -0.06 dex $\lesssim$ [Fe/H] $\lesssim 0.33$ dex.

Concluding, the broad metallicity range covered by the new Cepheids suggest that young and evolved stars in the two innermost Galactic regions with ongoing star formation activity, i.e. the ID and the nuclear bulge, have similar iron abundances, thus supporting a correlation between their chemical enrichment histories. On the other side, the absence of a clear azimuthal metallicity gradient rules out the dynamical effects of the bar's instabilities as the cause of the large observed metallicity spread. Thus, this dispersion seems then to be an intrinsic feature of the chemical composition of the Galactic ID, suggesting that its metallicity distribution cannot be modelled by using one-dimensional gradients.

This work shows that our understanding of the central regions of the Galaxy is still severely biased by the limited number of tracers available. Deep photometric surveys, especially in the NIR, together with NIR follow-up spectroscopy are necessary to achieve more firms conclusions on the topic. By succeeding in performing the spectroscopic analysis of NIR spectra for pulsating supergiant stars we contribute to make one step farther in this direction.

ACKNOWLEDGEMENTS

REFERENCES

Allard E. L., Knapen J. H., Peletier R. F., Sarzi M., 2006, MNRAS, 371, 1087

Anderson R. I., 2016, MNRAS, 463, 1707

Andrievsky S. M., Bersier D., Kovtyukh V. V., Luck R. E., Maciel W. J., Lépine J. R. D., Beletsky Y. V., 2002, A&A, 384, 140

Andrievsky S. M., Martin R. P., Kovtyukh V. V., Korotin S. A., Lépine J. R. D., 2016, MNRAS, 461, 4256

Athanassoula E., 1992, MNRAS, 259, 345

Baba J., Kawata D., Matsunaga N., Grand R. J. J., Hunt J. A. S., 2018, ApJ, 853, L23

Bally J. et al., 2010, A&A, 518, L90

Benjamin R. A. et al., 2005, ApJ, 630, L149

Beuther H., Meidt S., Schinnerer E., Paladino R., Leroy A., 2017, A&A, 597, A85

Bhardwaj A., Macri L. M., Rejkuba M., Kanbur S. M., Ngeow C.-C., Singh H. P., 2017, AJ, 153, 154

Bland-Hawthorn J., Gerhard O., 2016, ARA&A, 54, 529

Bobylev V. V., Bajkova A. T., 2015, Astron. Lett., 41, 473

Bono G., Castellani V., Marconi M., 2002, ApJ, 565, L83

Bono G., Marconi M., Cassisi S., Caputo F., Gieren W., Pietrzynski G., 2005, ApJ, 621, 966

Bovy J. et al., 2014, ApJ, 790, 127

Bovy J., Rix H.-W., Green G. M., Schlafly E. F., Finkbeiner D. P., 2016, ApJ, 818, 130

Cardelli J. A., Clayton G. C., Mathis J. S., 1989, ApJ, 345, 245

Chiappini C., Matteucci F., Gratton R., 1997, ApJ, 477, 765

Cunha K., Sellgren K., Smith V. V., Ramirez S. V., Blum R. D., Terndrup D. M., 2007, ApJ, 669, 1011

da Silva R. et al., 2016, A&A, 586, A125

Daflon S., Cunha K., 2004, ApJ, 617, 1115

Davies B., Origlia L., Kudritzki R.-P., Figer D. F., Rich R. M., Najarro F., 2009a, ApJ, 694, 46

Davies B., Origlia L., Kudritzki R.-P., Figer D. F., Rich R. M., Najarro F., Negueruela I., Clark J. S., 2009b, ApJ, 696, 2014

Debattista V. P., Ness M., Gonzalez O. A., Freeman K., Zoccali M., Minniti D., 2017, MNRAS, 469, 1587

Dékány I. et al., 2015a, ApJ, 799, L11

Dékány I. et al., 2015b, ApJ, 812, L29

Drimmel R., Spergel D. N., 2001, ApJ, 556, 181

Drimmel R., Cabrera-Lavers A., López-Corredoira M., 2003, A&A, 409, 205

Feast M., Whitelock P., 1997, MNRAS, 291, 683

Feltzing S., Chiba M., 2013, New Astron. Rev., 57, 80

Friedli D., Benz W., 1995, A&A, 301, 649

Genovali K. et al., 2013, A&A, 554, A132

Genovali K. et al., 2014, A&A, 566, A37

Groenewegen M. A. T., Udalski A., Bono G., 2008, A&A, 481, 441

Hamano S. et al., 2016, ApJ, 821, 42

Heyer M., Dame T. M., 2015, ARA&A, 53, 583

Hunt J. A. S., Kawata D., Monari G., Grand R. J. J., Famaey B., Siebert A., 2017, MNRAS, 467, L21

Inno L. et al., 2015, A&A, 576, A30

Inno L. et al., 2016, ApJ, 832, 176

Jacobson H. R. et al., 2016, A&A, 591, A37

Joblin C., D'Hendecourt L., Leger A., Maillard J. P., 1990, Nature, 346, 729

Kato D. et al., 2007, PASJ, 59, 615

Khoperskov S., Di Matteo P., Haywood M., Combes F., 2018, A&A, 611, L2

Kim S. S., Saitoh T. R., Jeon M., Figer D. F., Merritt D., Wada K., 2011, ApJ, 735, L11

Kovtyukh V. V., Chekhonadskikh F. A., Luck R. E., Soubiran C., Yasinskaya M. P., Belik S. I., 2010, MNRAS, 408, 1568

Kovtyukh V. et al., 2016, MNRAS, 460, 2077

Laney C. D., Stobie R. S., 1992, A&AS, 93, 93

Lemasle B., François P., Bono G., Mottini M., Primas F., Romaniello M., 2007, A&A, 467, 283

Lemasle B., François P., Piersimoni A., Pedicelli S., Bono G., Laney C. D., Primas F., Romaniello M., 2008, A&A, 490, 613

Lépine J. R. D., Roman-Lopes A., Abraham Z., Junqueira T. C., Mishurov Y. N., 2011, MNRAS, 414, 1607

Luck R. E., Lambert D. L., 2011, AJ, 142, 136

Luck R. E., Andrievsky S. M., Kovtyukh V. V., Gieren W., Graczyk D., 2011, AJ, 142, 51

Macri L. M., Ngeow C.-C., Kanbur S. M., Mahzooni S., Smitka M. T., 2015, AJ, 149, 117

Majaess D., Turner D., Dékány I., Minniti D., Gieren W., 2016, A&A, 593, A124

Martin R. P., Andrievsky S. M., Kovtyukh V. V., Korotin S. A., Yegorova I. A., Saviane I., 2015, MNRAS, 449, 4071

Matsunaga N., Kawadu T., Nishiyama S., Nagayama T., Hatano H., Tamura M., Glass I. S., Nagata T., 2009, MNRAS, 399, 1709

Matsunaga N. et al., 2011, Nature, 477, 188

Matsunaga N. et al., 2013, MNRAS, 429, 385

Matsunaga N. et al., 2015, ApJ, 799, 46

Matsunaga N. et al., 2016, MNRAS, 462, 414

Matsunaga N., Bono G., Chen X., de Grijs R., Inno L., Nishiyama S., 2018, Space Sci. Rev., 214, 74

Meidt S. E. et al., 2018, ApJ, 854, 100

Metzger M. R., Schechter P. L., 1998, AJ, 116, 469

Minchev I., Chiappini C., Martig M., 2013, A&A, 558, A9

Minniti D. et al., 2010, New Astron., 15, 433

Monson A. J., Pierce M. J., 2011, ApJS, 193, 12

Nagashima C. et al., 1999, in Nakamoto T., ed. Star Formation 1999. Nobeyama Radio Observatory, p. 397

Nagayama T. et al., 2003, in Iye M., Moorwood A. F. M., eds, Proc. SPIE Conf. Ser. Vol. 4841, Instrument Design and Performance for Optical/Infrared Ground-based Telescopes. SPIE, Bellingham, p. 459

Najarro F., Figer D. F., Hillier D. J., Geballe T. R., Kudritzki R. P., 2009, ApJ, 691, 1816

Nardetto N., Fokin A., Fouqué P., Storm J., Gieren W., Pietrzynski G., Mourard D., Kervella P., 2011, A&A, 534, L16

Nataf D. M. et al., 2016, MNRAS, 456, 2692

Nishiyama S. et al., 2006, ApJ, 638, 839

Origlia L. et al., 2013, A&A, 560, A46

Pedicelli S. et al., 2010, A&A, 518, A11

Persson S. E., Madore B. F., Krzemiński W., Freedman W. L., Roth M., Murphy D. C., 2004, AJ, 128, 2239

Pietrzyński G. et al., 2013, Nature, 495, 76

Proxauf B., 2017, Master thesis

Reid M. J. et al., 2009, ApJ, 700, 137

Reid M. J. et al., 2014, ApJ, 783, 130

Reid M. J., Dame T. M., Menten K. M., Brunthaler A., 2016, ApJ, 823, 77

Rieke G. H., Lebofsky M. J., 1985, ApJ, 288, 618

Rix H.-W., Bovy J., 2013, A&AR, 21, 61

Ryde N., Schultheis M., 2015, A&A, 573, A14

Sánchez-Blázquez P., Ocvirk P., Gibson B. K., Pérez I., Peletier R. F., 2011, MNRAS, 415, 709

Sasselov D. D., Lester J. B., 1990, ApJ, 362, 333

Schlafly E. F. et al., 2016, ApJ, 821, 78

Shetty R., Vogel S. N., Ostriker E. C., Teuben P. J., 2007, ApJ, 665, 1138

Simon N. R., Lee A. S., 1981, ApJ, 248, 291

Skrutskie M. F. et al., 2006, AJ, 131, 1163

Sormani M. C., Treß R. G., Ridley M., Glover S. C. O., Klessen R. S., Binney J., Magorrian J., Smith R., 2018, MNRAS, 475, 2383

Soszyński I. et al., 2018, Acta Astron., 68, 89

Spina L. et al., 2017, A&A, 601, A70

Stetson P. B., 1987, PASP, 99, 191

Storm J. et al., 2011a, A&A, 534, A94

Storm J., Gieren W., Fouqué P., Barnes T. G., Soszyński I., Pietrzyński G., Nardetto N., Queloz D., 2011b, A&A, 534, A95

Sziládi K., Vinkó J., Poretti E., Szabados L., Kun M., 2007, A&A, 473, 579

Tanioka S., Matsunaga N., Fukue K., Inno L., Bono G., Kobayashi N., 2017, ApJ, 842, 104

Urbaneja M. A., Kudritzki R.-P., Gieren W., Pietrzyński G., Bresolin F., Przybilla N., 2017, AJ, 154, 102

Vallée J. P., 2017, Ap&SS, 362, 173

VanderPlas J. T., 2018, ApJS, 236, 16

VanderPlas J. T., Ivezić Ž., 2015, ApJ, 812, 18

Windmark F., Lindegren L., Hobbs D., 2011, A&A, 530, A76

Yong D., Carney B. W., Teixera de Almeida M. L., Pohl B. L., 2006, AJ, 131, 2256

Zaritsky D., Kennicutt R. C., Jr, Huchra J. P., 1994, ApJ, 420, 87

This paper has been typeset from a TEX/LATEX file prepared by the author.